Hindawi
Adsorption Science & Technology
Volume 2022, Article ID 2248249, 16 pages
https://doi.org/10.1155/2022/2248249

Research Article

Sulfhydryl Functionalized Magnetic Chitosan as an Efficient Adsorbent for High-Performance Removal of Cd(II) from Water: Adsorption Isotherms, Kinetic, and Reusability Studies

Jari S. Algethami,[1] **Ayoub Abdullah Alqadami**,[2] **Saad Melhi**,[3] **Mohsen A. M. Alhamami**,[1] **Ahmed M. Fallatah**,[4] **and Moustafa A. Rizk**[5,6]

[1]*Department of Chemistry, College of Science and Arts, Najran University, P.O. Box, 1988, Najran 11001, Saudi Arabia*
[2]*Department of Chemistry, College of Science, King Saud University, Riyadh 11451, Saudi Arabia*
[3]*Department of Chemistry, College of Science, University of Bisha, Bisha, 61922, Saudi Arabia*
[4]*Department of Chemistry, College of Science, Taif University, P. O. Box 11099, Taif 21944, Saudi Arabia*
[5]*Department of Chemistry, College of Science and Arts at Sharurah, Najran University, Najran 11001, Saudi Arabia*
[6]*Department of Chemistry of Science Faculty, Suez Canal University, Ismailia 41522, Egypt*

Correspondence should be addressed to Ayoub Abdullah Alqadami; aalkudami@ksu.edu.sa
and Moustafa A. Rizk; marizk@nu.edu.sa

Received 20 April 2022; Accepted 16 May 2022; Published 13 June 2022

Academic Editor: Hassan M. Hassan

In this study, dimercaptosuccinic acid-functionalized magnetic chitosan (Fe_3O_4@CS@DMSA) was synthesized via in situ coprecipitation process and amidation reaction, aiming to eliminate cadmium (Cd(II)) ions from an aqueous environment. The structure, morphology, and particle size of the Fe_3O_4@CS@DMSA adsorbent were investigated using FTIR, TEM, EDX, TGA, zeta potential, and XRD techniques, and the obtained results approved the successful synthesis of the Fe_3O_4@CS@DMSA nanocomposite. The influence of external adsorption conditions such as pH solution, adsorbent mass, initial Cd(II) concentration, temperature, and contact time on the adsorption process was successfully achieved. Accordingly, pH: 7.6, contact time: 210 min, and adsorbent mass:10 mg were found to be the optimal conditions for best removal. The adsorption was analyzed using nonlinear isotherm and kinetic models. The outcomes revealed that the adsorption process obeyed the Langmuir and the pseudo-first-order models. The maximum adsorption capacity of Fe_3O_4@CS@DMSA toward Cd(II) ion was 314.12 mg/g. The adsorption mechanism of Cd(II) on Fe_3O_4@CS@DMSA nanocomposite is the electrostatic interaction. The reusability test of Fe_3O_4@CS@DMSA nanocomposite exhibited that the adsorption efficiency was 72% after the 5th cycle. Finally, this research indicates that the Fe_3O_4@CS@DMSA exhibited excellent characteristics such as high adsorption capacity, effective adsorption-desorption results, and easy magnetic separation and thus could be an effective adsorbent for removing Cd(II) ions from aqueous solutions.

1. Introduction

Water contamination by a toxic cadmium (Cd(II)) metal is a widespread environmental issue owing to its long-term adverse effects on humans and ecosystems. Cd(II) is one of the most dangerous metal ion due to its nondegradable, strong bioaccumulate, and highly toxic even at low concentrations, which leads to a serious threat to human health [1, 2]. Cd(II) pollution can cause kidney, liver, and bone damage to humans with a long time exposure. Cd(II) has excellent solubility which can be easily released into the aqueous systems through industrial production processes such as alkaline batteries, electroplating, textile printing industries, and pigment [3]. Cd(II) is classified as a category one carcinogen by U.S. EPA, and the maximum concentration of Cd(II) in drinking water is 5 μg/L [4, 5]. Thus, the

removal of extremely toxic cadmium from an aqueous environment is essential to avoid pollution to the environmental systems. Several techniques, namely, chemical precipitation [6], adsorption [7], membrane separation [8], ion exchange [9], and electrodeposition [10, 11], have been applied to treat the toxic metals from wastewater. Among them, the adsorption technique has been proven economical, simple, easy operation and ecofriendly, cost-effective, versatile in nature, and highly efficient for metal removal [12].

Many adsorbents have been applied to adsorption of Cd(II) from aqueous medium like sulfonated biochar [13], functionalized cellulose derived [14], amino-functionalized lignin [15], metal-organic framework (MOF) ZIF-8 [16], EDTA/mGO [17], and para-aminobenzoic acid-functionalized activated [18]. These adsorbents suffer from the difficulty of recovering metal after adsorption using traditional methods such as centrifugation and filtration, which may result in secondary pollution and loss of the amount of adsorbents [19]. Magnetic nanocomposite has received great attention as an efficient adsorbent owing to its many advantages such as easy magnetic separation, high surface area, low toxicity, biocompatibility, and the existence of a large number of surface hydroxyl groups that use them in surface modification. To improve the stability of Fe_3O_4 nanoparticles under acidic conditions and reduce the agglomeration of the nanoparticles, the surface of Fe_3O_4 nanoparticles can be modified with some materials like activated carbon [20], graphite oxide [21], and carboxylated MNP nanoparticles [22].

Naturally abundant polysaccharides such as chitosan are considered as one of the most promising surface stabilizing materials for magnetite nanoparticles due to their multifunctionality, nontoxicity, biocompatibility, and renewability [23]. Chitosan has a strong affinity with metal ions because of the existence of NH_2 and OH groups which can serve as the active adsorption sites for the removal of metals [24–26]. To improve the number of active adsorption sites for adsorption on magnetic chitosan, it needs to be surface modified to provide specific functional groups. Meso-2,3-dimercaptosuccinic acid (DMSA) is a suitable candidate for enhancing the adsorption process owing to DMSA having carboxyl and thiol groups, which can be used for the capture of heavy metals [27, 28]. In addition, DMSA acid is a nontoxic chelating agent and FDA approved drug which has been used to treat heavy metal poisoning in the human body [29–31]. To the best of our knowledge, the Fe_3O_4@CS@DMSA nanocomposite has not been used for the elimination of pollutants.

In this study, Fe_3O_4@CS@DMSA nanocomposite was synthesized by an in situ coprecipitation method followed by a covalent functionalization of Fe_3O_4@CS with DMSA acid via amidation reaction. The synthesized Fe_3O_4@CS@DMSA adsorbent was applied to eliminate Cd(II) ions from water. The synthesized Fe_3O_4@CS@DMSA was characterized using zeta potential, FTIR, XRD, TGA, TEM, and EDX techniques. The impact of external adsorption conditions such as pH solution, adsorbent mass, initial Cd(II) concentration, temperature, and contact time on the adsorption process was successfully achieved. To achieve the adsorption capacity and mechanisms of Cd(II) adsorption onto Fe_3O_4@CS@DMSA nanocomposite, the equilibrium kinetic and isotherm were studied. Thermodynamic parameters were also studied. The reusability test of Fe_3O_4@CS@DMSA nanocomposite was performed by carrying out five cycles of adsorption-desorption studies.

2. Experimental

2.1. Chemicals and Reagents. $FeCl_2{\cdot}4H_2O$, ≥99%, $FeCl_3{\cdot}6H_2O$, ≥99%, chitosan, medium MW, meso-2,3-dimercaptosuccinic acid, ~98%, and 1-ethyl-3-(3-dimethylaminopropyl)carbodiimide (EDC) were purchased from Sigma-Aldrich, USA. Dimethyl sulfoxide (DMSO) was obtained from Panreac, UK. HNO_3, 69%, NaOH, ≥98%, and $Cd(NO_3)_2$ were obtained from BDH Chemicals Ltd. (Poole, England). NH_4OH, 25%, and HCl, 36.5-38%, were procured from Merck, Germany. All chemicals and reagents utilized in these experiments were of AR grade.

2.2. Synthesis of Fe_3O_4@CS. Magnetic chitosan (Fe_3O_4@CS) was synthesized by an in situ coprecipitation method according to the literature [32] with some modifications. Typically, 1.8 g of chitosan (CS) was dissolved in acetic acid solution (100 mL, 3% w/w) under magnetic stirring and N_2 gas. Then, the chitosan solution was transferred into a three-necked-round bottom flask containing $FeCl_2{\cdot}4H_2O$ (2.98 g) and $FeCl_3{\cdot}6H_2O$ (8.11 g) with a molar ratio (1 : 2). The mixture was stirred mechanically at 75°C for 15 min, and then, 35 mL of ammonia (25 wt%) was added to the mixture dropwise until pH reaches 10. After mechanical stirring for another 120 min, the precipitate was cooled at room temperature and then was collected by a magnet. Finally, the Fe_3O_4@CS was washed with deionized water and then dried at 50°C for 24 h. A brief preparation procedure of Fe_3O_4@CS is demonstrated in Scheme 1.

2.3. Synthesis of Fe_3O_4@CS@DMSA. Fe_3O_4@CS@DMSA nanocomposite was synthesized by amidation reaction between the carboxylic group of DMSA and the amino group of magnetic chitosan (Fe_3O_4@CS). Typically, DMSA (0.91 g) was added into 50 mL of DMSO to be completely dissolved by ultrasonication; then, 0.776 g of EDC was added into the DMSA solution under ultrasonication and N_2 gas for 1.0 h. After that, 1.00 g of Fe_3O_4@CS was dispersed into the above solution by mechanical stirring under N_2 gas for 24 h. Then, the black product was isolated by a magnet and then washed with D.I. water. Finally, the Fe_3O_4@CS@DMSA was dried at 50°C for 24 h. A brief preparation procedure of Fe_3O_4@CS@DMSA is demonstrated in Scheme 1.

2.4. Characterization of Fe_3O_4@CS@DMSA Nanocomposite. The functional groups of Fe_3O_4 nanoparticles, DMSA, Fe_3O_4@CS@DMSA, and Cd(II)-loaded Fe_3O_4@CS@DMSA were recorded by Fourier transform infrared spectroscopy (FTIR) (Nicolet 6700, Thermo Scientific, USA). The morphology and particle size of the Fe_3O_4@CS@DMSA were performed using TEM (JEOL 2100, Japan). The surface composition of Fe_3O_4@CS@DMSA and Cd(II)-loaded Fe_3O_4@CS@DMSA was analyzed by energy-dispersive X-ray (EDX) using EDXS: AMETEK Nova 200. The crystallinity nature of Fe_3O_4 nanoparticles and Fe_3O_4@CS@DMSA

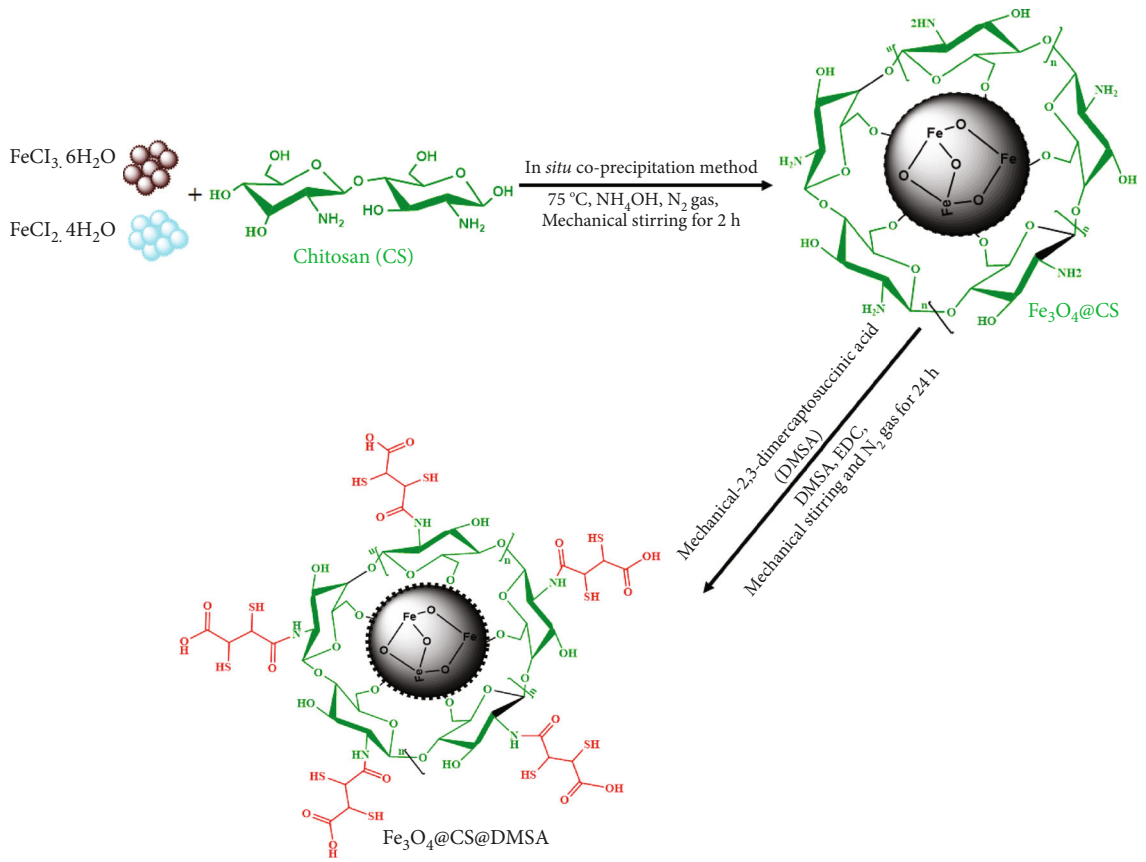

Scheme 1: Schematic for preparation of Fe_3O_4@CS@DMSA nanocomposite.

nanocomposite was performed by XRD analysis using a Shimadzu model 6000. The zeta potential of Fe_3O_4@CS@DMSA nanocomposite was determined using a Nano Plus Series, USA. TGA curve was recorded Fe_3O_4@CS@DMSA nanocomposite using a thermogravimetric analyzer (Mettler Toledo GA/SDTA851) under an N_2 atmosphere.

2.5. Batch Adsorption Experiments. The removal efficiency of Cd(II) ions by Fe_3O_4@CS@DMSA from water was studied by batch method to achieve the impact of various process factors such as adsorbent mass, contact time, pH solution, temperature, and initial Cd(II) concentration on adsorption process. In this work, contact time, solution pH, and adsorbent mass were achieved in the range of 5-350 min, 1.8-9.1, and 5-30 mg whereas temperature and initial Cd(II) concentration were varied from 25 to 45°C and 25 to 300 mg/L. A known amount of Fe_3O_4@CS@DMSA was put into an Erlenmeyer containing 25 mL of known Cd(II) concentration, and the sample was then adjusted to the desired pH at 25°C. After that, the sample solution was shaken for 24 h. Then, the sample was isolated by a magnet, and the residual concentration of Cd(II) ions has been determined using AAS. The adsorbed amount (q_e (mg/g)) and percentage adsorption of Cd(II) were calculated using Equations (1) and (2), respectively.

$$q_e = (C_o - C_e)\frac{V}{m}, \tag{1}$$

$$\%\text{adsorption} = \frac{C_o - C_e}{C_o} \times 100, \tag{2}$$

where C_o and C_e refer to initial and equilibrium Cd(II) concentration in the solution (mg/L), respectively; V (L) refers to the volume of the Cd(II) solution; m (g) is the weight of Fe_3O_4@CS@DMSA nanocomposite. The adsorption capacities for Fe_3O_4@CS and Fe_3O_4@CS@DMSA adsorbents toward Cd(II) ions were 52.5 mg/g and 58.8 mg/g, respectively, at condition parameters at constant adsorbent mass (0.01 g), initial Cd(II) concentration (25 mg/L), temperature (25°C), pH (7.6), stirring rate (100 rpm), and contact time (1440 min).

3. Results and Discussion

3.1. Characterization of Fe_3O_4@CS@DMSA Nanocomposite. Figure 1(a) shows the FTIR spectra of Fe_3O_4 nanoparticles, DMSA, Fe_3O_4@CS@DMSA, and Cd(II)-loaded Fe_3O_4@CS@DMSA. For Fe_3O_4 nanoparticles, the characteristic bands at 572 and 1612 cm^{-1} are due to the Fe –O and –OH bonds, respectively [33]. In the spectrum of DMSA, the characteristic bands are shown at around 2551 and 1693 cm^{-1} attributed to ν(-SH) and ν(COOH) groups, respectively [34, 35]. The bands 3520, 2983, 1413, 1296, and 1175 cm^{-1} are due to the stretching vibration of ν(-OH), ν(-CH), ν(-COO-), ν(C-O), and ν(O-C-O) bonds, respectively [34]. For Fe_3O_4@CS@DMSA, the bands at 3393 cm^{-1} are attributed

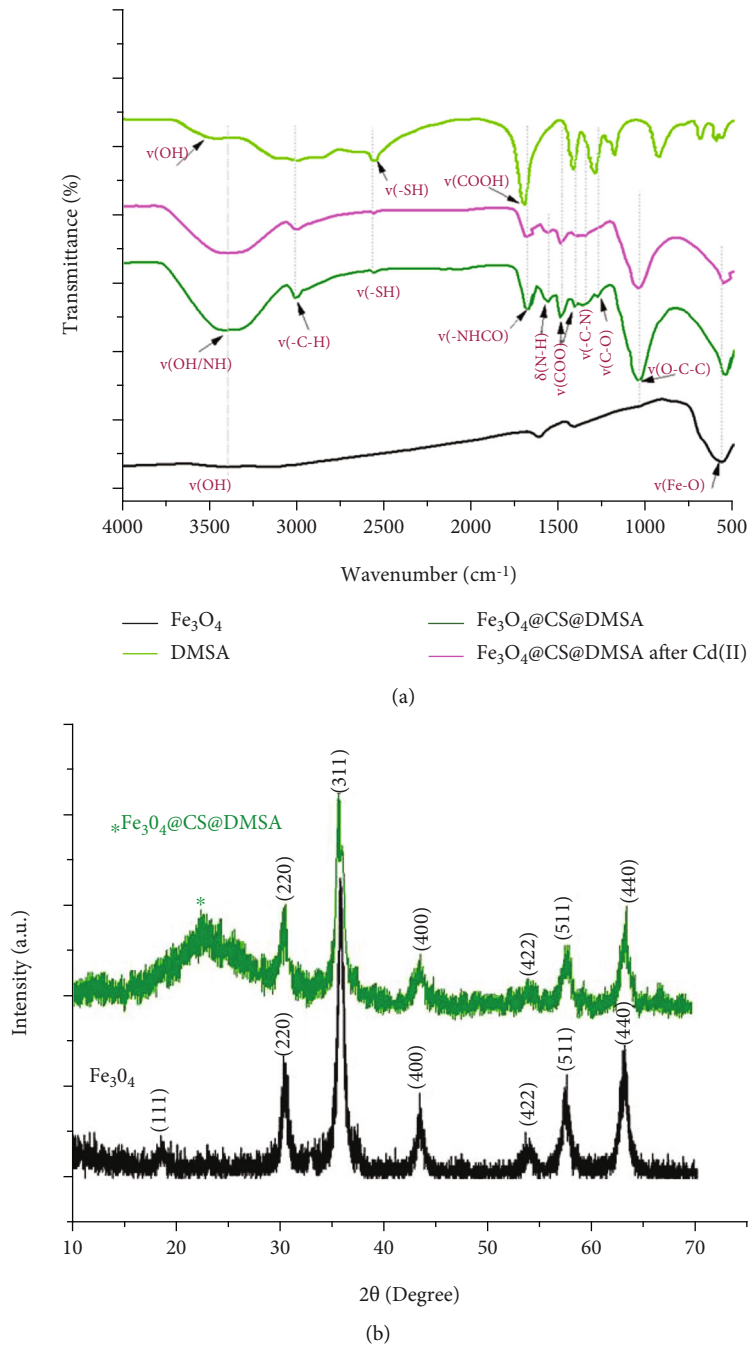

Figure 1: FTIR spectra of (a) Fe_3O_4, DMSA, Fe_3O_4@CS@DMSA, and Cd(II)-loaded Fe_3O_4@CS@DMSA and (b) XRD pattern of Fe_3O_4, and Fe_3O_4@CS@DMSA.

to the presence of the ν(-OH) group overlapping with the -NH group. The characteristic band for (–SH) appeared at 2550 cm^{-1} [34]. Besides, the bands at 1670 and 1554 cm^{-1} are due to amide I and amide II or δ(N–H) groups, respectively [36], which indicates the formation of amide bonds between Fe_3O_4@CS and DMSA [37]. The Fe-O band was decreased to 552 cm^{-1}, confirming the presence of magnetic nanoparticles. The bands at 1481, 1355, 1274, and 1044 cm^{-1} are due to ν(-COO-), ν(-C-N), ν(C-O), and ν(O-C-O) stretching vibration, respectively [38, 39]. After adsorption of Cd(II), the spectra showed the bands were slightly shifted and decreased in intensity due to the binding of COOH, SH, and OH onto Fe_3O_4@CS@DMSA surface with Cd(II) ions through electrostatic attractions. In detail, the bands at 3393 and 2550 cm^{-1} decrease in intensity owing to the interaction between Cd(II) and carboxyl (COOH), hydroxyl (OH), and SH groups, respectively, on the Fe_3O_4@CS@DMSA surface by electrostatic interaction. In addition, the band at 1274 cm^{-1} for ν(C-O) disappeared after Cd(II) adsorption onto the Fe_3O_4@CS@DMSA surface. The decreased intensity of the band at 1481 cm^{-1} for $\nu(COO^-)$ indicates the adsorption of Cd(II) onto the Fe_3O_4@CS@DMSA surface.

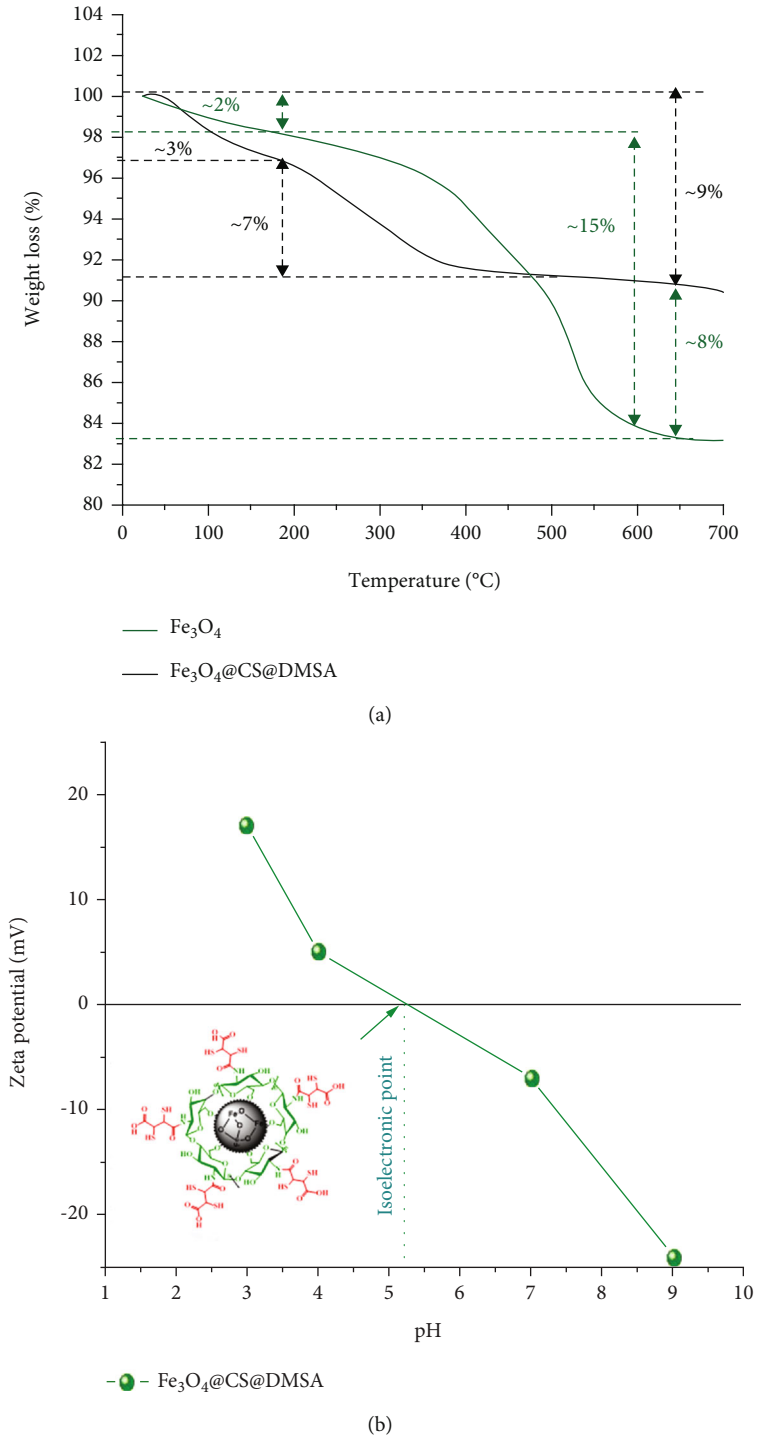

Figure 2: TGA analysis of (a) Fe_3O_4 and Fe_3O_4@CS@DMSA and (b) zeta potential plots as a function of Fe_3O_4@CS@DMSA nanocomposite.

The XRD patterns of magnetite nanoparticles and Fe_3O_4@CS@DMSA are indicated in Figure 1(b). The major peaks at $2\theta = 18.3^\circ$, 30.2°, 35.7°, 43.13°, 54.4°, 57.6°, and 63.3° are associated with the (111), (220), (311), (400), (422), (511), and (400) crystal planes of cubic phase magnetite, which was consistent with a previous report [40]. Compared with magnetite, the XRD pattern of Fe_3O_4@CS@DMSA appeared a new broad reflection at a 2θ value of 22.5°, confirming the Fe_3O_4 nanoparticles covered by DMSA and chitosan [41, 42]. Using the Scherer equation (3), the average crystal size (D) of Fe_3O_4@CS@DMSA nanocomposite was calculated:

$$D = \frac{k\lambda}{\beta \cos\theta}, \tag{3}$$

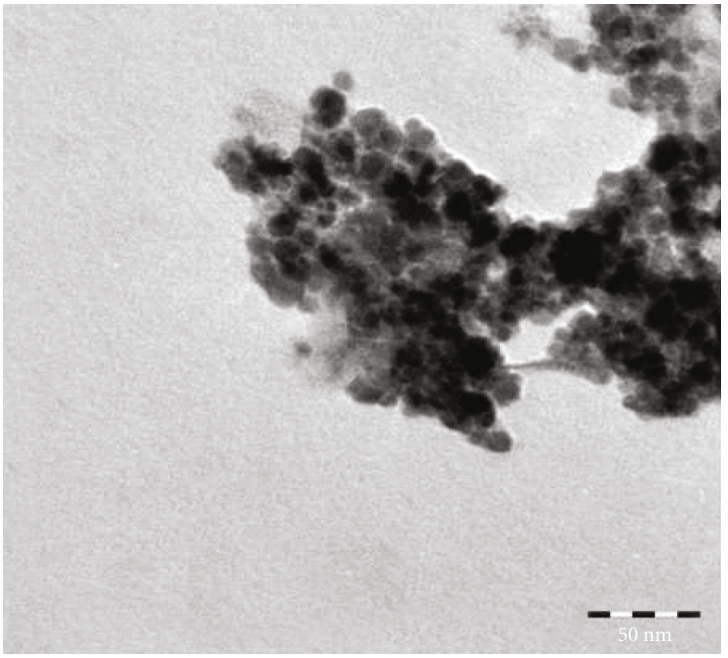

(a)

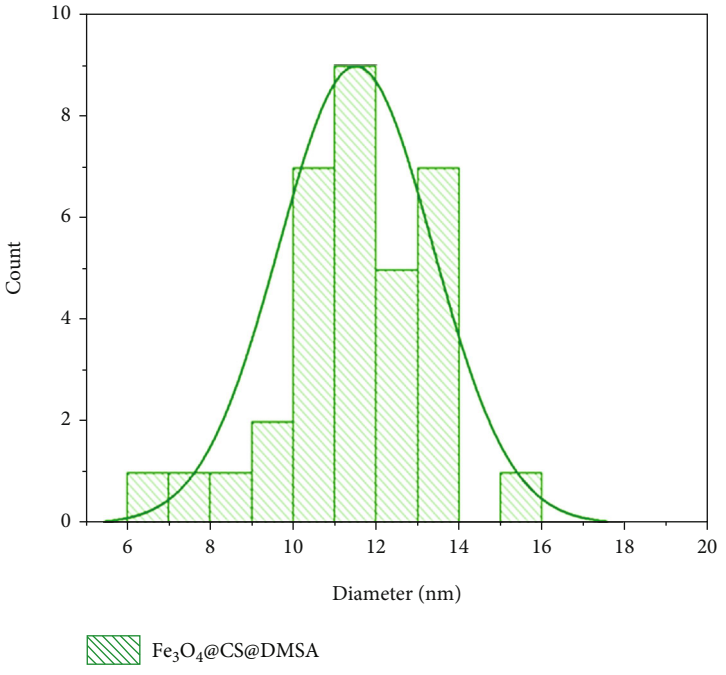

(b)

Figure 3: (a) TEM image and (b) particle size distribution plots of Fe_3O_4@CS@DMSA nanocomposite.

Table 1: EDX analysis.

Sample	Elemental content (weight %)					
	Fe	O	N	C	S	Cd
Fe_3O_4@CS@DMSA	59.82	21.38	1.17	16.61	1.02	0
Cd(II)-loaded Fe_3O_4@CS@DMSA	56.99	19.61	0.91	20.92	0.75	0.82

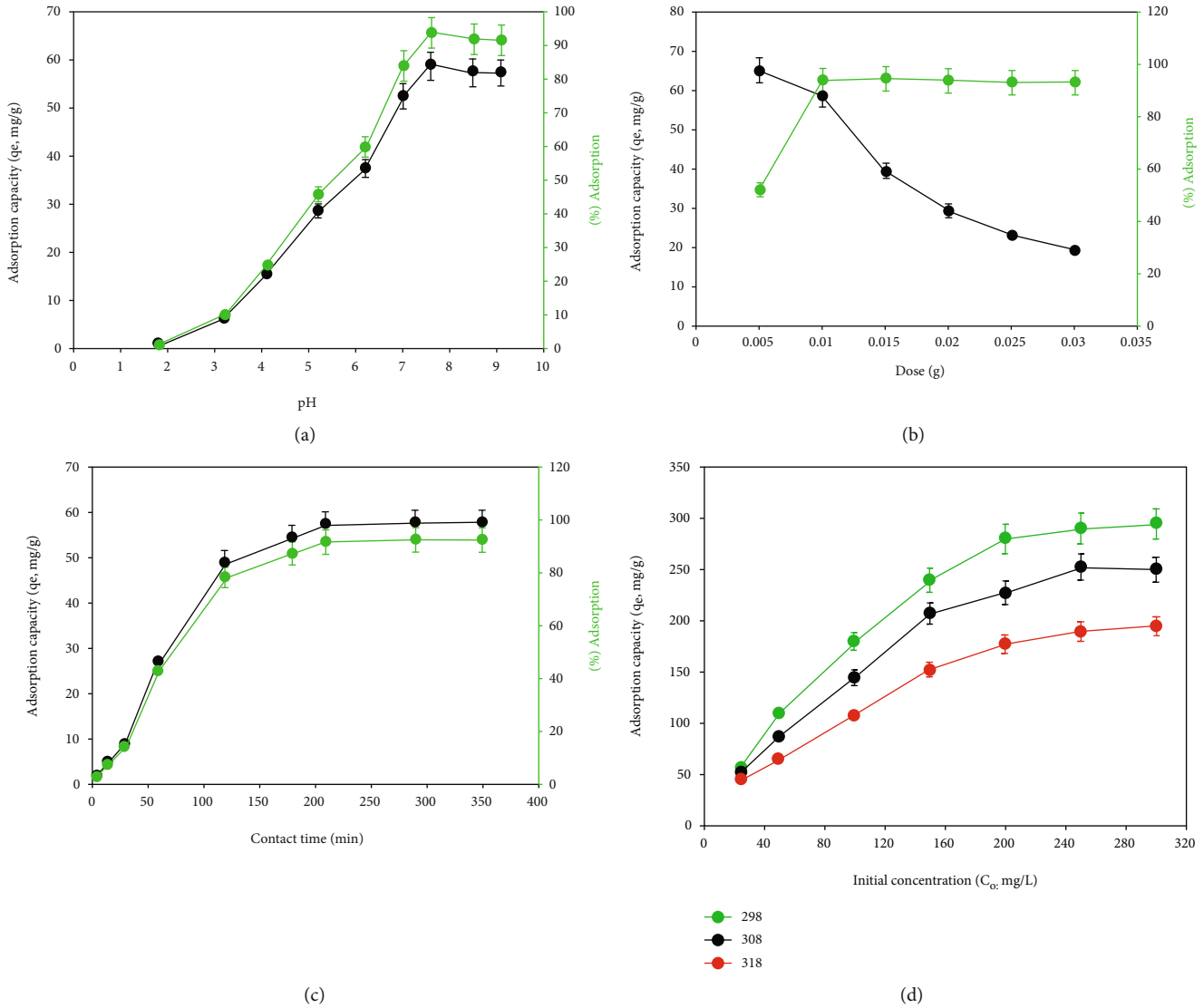

FIGURE 4: Effect of (a) pH (adsorbent dose: 0.01 g; C_o: 25 mg/L; agitation speed: 100 rpm; time: 1440 min), (b) adsorbent dose (T: 298 K; C_o: 25 mg/L; T: 298 K; time: 1440 min; agitation speed: 100 rpm), (c) contact time (adsorbent dose: 0.01 g; C_o: 25 mg/L; T: 298 K; agitation speed: 100 rpm), and (d) initial Cd(II) concentration on adsorption of Cd(II) by Fe_3O_4@CS@DMSA (T: 298-318 K; adsorbent dose: 0.01 g; agitation speed: 100 rpm).

where $\lambda = 0.154$ nm is the X-ray wavelength; θ is Bragg's peak; β is the half-width of diffraction peak; K is the Scherer constant. The mean crystal size of Fe_3O_4@CS@DMSA nanocomposite was 11.5 nm.

Figure 2(a) displays the TGA curves for Fe_3O_4 nanoparticles and Fe_3O_4@CS@DMSA nanocomposite. The total weight loss was ~9% and 17% observed for Fe_3O_4 nanoparticles and Fe_3O_4@CS@DMSA nanocomposite, respectively. The weight loss of mass for magnetite nanoparticles in a range of temperatures (30-700°C) due to evaporation of adsorbed H_2O and decomposition of oxygen-containing functional groups from the Fe_3O_4 nanoparticles [43, 44]. The thermal stability of Fe_3O_4@CS@DMSA exhibited a high loss in mass of approximately 17% with two stages. In the first one, the weight loss was ~3% in low temperature up to 200°C owing to elimination of adsorbed water and solvent absorbed onto the surface Fe_3O_4@CS@DMSA nanocomposite. In the second one, ~15% weight loss at around 200–700°C ascribes to the thermal decomposition of an organic part of CS and DMSA [45], confirming the successful synthesis of Fe_3O_4@CS@DMSA nanocomposites.

To determine the point of zero charge (PZC) of Fe_3O_4@CS@DMSA, the surface charge of Fe_3O_4@CS@DMSA was measured under different pH values. The outcomes are displayed in Figure 2(b). It was seen that the zero of point charge value (pH_{pzc}) of Fe_3O_4@CS@DMSA nanocomposite was ~5.2. This value is lower than ~7.1 for Fe_3O_4 nanoparticles [46]. This behavior of the Fe_3O_4@CS@DMSA nanocomposite is mainly assigned to the existence of –OH, COOH, and –SH groups, which are being protonated at lower than ~5.2.

The size and morphology of the Fe_3O_4@CS@DMSA were studied by TEM, and the outcomes are displayed in

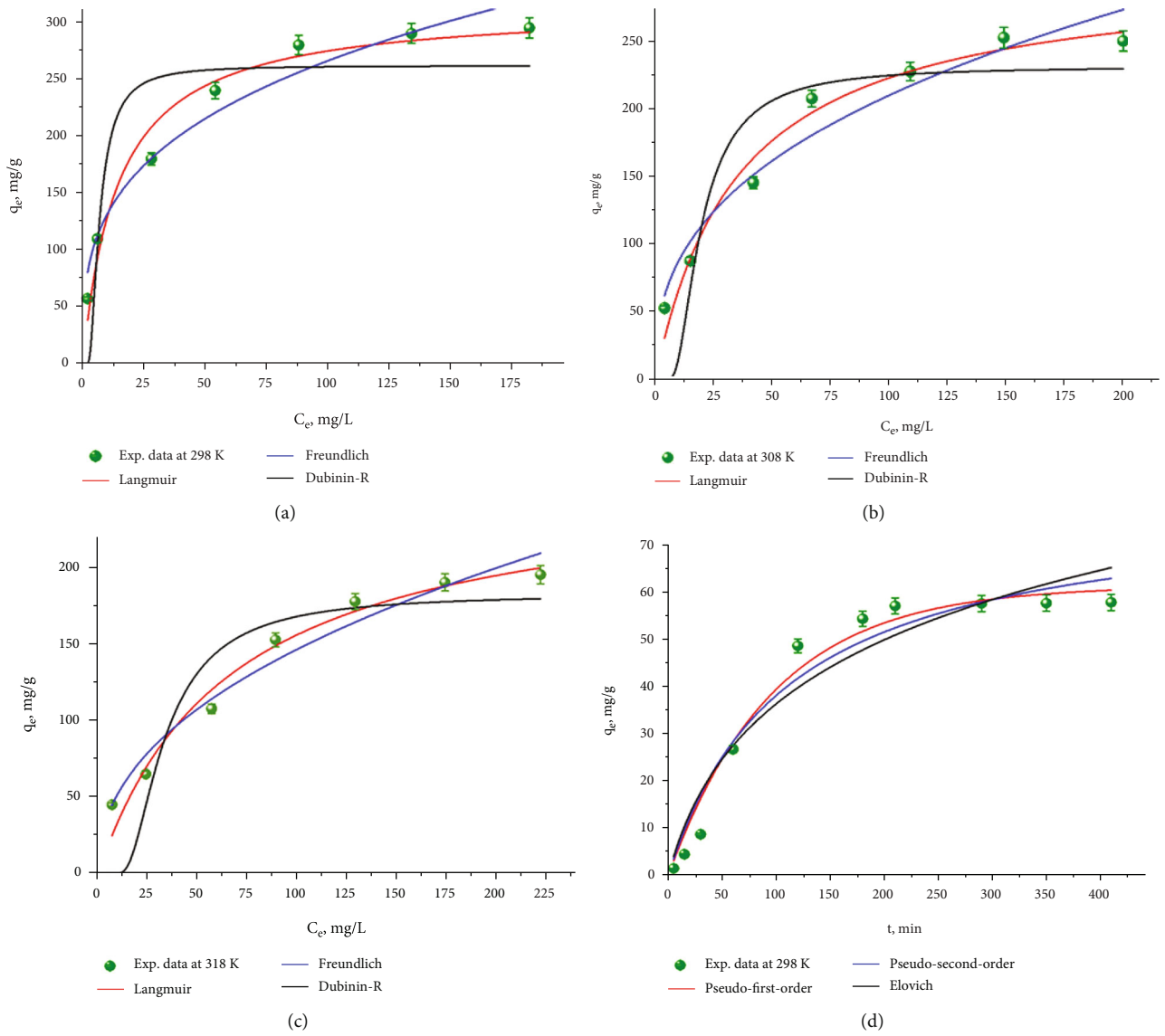

FIGURE 5: Adsorption isotherm fit for the Cd(II) adsorption onto Fe_3O_4@CS@DMSA at (a) 298 K, (b) 303 K, and (c) 318 (time: 210 min; C_o: 25-300 mg/L; adsorbent dose: 0.01 g; agitation speed: 100 rpm); adsorption kinetic fit for the Cd(II) adsorption onto Fe_3O_4@CS@DMSA at (d) 298 K (T: 298 K; C_o: 25 mg/L; adsorbent dose: 0.01 g; agitation speed: 100 rpm).

Figure 3(a). It is clear that the nanoparticles were uniform spherical morphology with a bright of amorphous CS and DMSA over the dark spot crystalline core of magnetite nanoparticles [47]. The value particle size of Fe_3O_4@CS@DMSA was ~11.5 nm confirming the surface modification of magnetite nanoparticles with CS and DMSA (Figure 3(b)). The elemental surface of Fe_3O_4@CS@DMSA and Cd(II)-saturated Fe_3O_4@CS@DMSA nanocomposite is shown in Table 1. The EDX analysis of Fe_3O_4@CS@DMSA showed the presence of Fe, O, C, N, and S on the Fe_3O_4@CS@DMSA surface, confirming the successfully prepared Fe_3O_4@CS@DMSA nanocomposite. The Cd(II) ions were observed on the Fe_3O_4@CS@DMSA surface after adsorption by EDX analysis (Table 1), which indicated the good adsorption capability of the Fe_3O_4@CS@DMSA nanocomposite when applied to Cd(II) adsorption.

3.2. Adsorption Study

3.2.1. Effect of pH Solution. The functional groups on the surface of Fe_3O_4@CS@DMSA nanocomposite and the state of Cd(II) metal ions are greatly influenced by H^+ concentration [48]. The effect of different initial pH values (1.8-9.1) on Cd(II) adsorption by Fe_3O_4@CS@DMSA nanocomposite was studied as shown in Figure 4(a). The other parameters were kept constant as initial Cd(II) concentration (25 mg/L), temperature (25°C), contact time (210 min), adsorbent mass (10 mg), and agitation speed (100 rpm). As implied in Figure 4(a), the adsorption capacity of Fe_3O_4@CS@DMSA toward Cd(II) was increased from 0.75 to 58.75 mg/g as the pH increased from 1.8 to 7.6, respectively. After that, it is slightly reduced and may be owing to the formation of Cd(II) hydroxide precipitate such as $Cd(OH)^+$ and $Cd(OH)_2$,

inhibiting the Cd(II) ion adsorption on Fe_3O_4@CS@DMSA nanocomposite [49–51]. The maximum value of Cd(II) elimination occurred at near pH (7.6). The zero-point charge of Fe_3O_4@CS@DMSA nanocomposite was determined as 5.2 as shown in Figure 2(b). Therefore, when the value of pH solution was lower than the pH_{zpc} (5.2), the surface of Fe_3O_4@CS@DMSA becomes positively charged and would form electrostatic repulsion between Fe_3O_4@CS@DMSA adsorbent and Cd(II) ions, which lead to reduced adsorption capacity. As the value of pH solution is greater than pH_{pzc} (5.2), the surface charge of Fe_3O_4@CS@DMSA nanocomposite becomes negatively charged, indicating the presence of electrostatic attraction between Cd(II) ions and Fe_3O_4@CS@DMSA nanocomposite which results in increased adsorption capacity. The pH = 7.6 was chosen as the optimum value for Cd(II) adsorption onto Fe_3O_4@CS@DMSA nanocomposite in this work.

3.2.2. Effect of Adsorbent Mass. Figure 4(b) demonstrates the Cd(II) adsorption onto Fe_3O_4@CS@DMSA nanocomposite under various adsorbent mass in the range between 5 mg and 30 mg at constant temperature (25°C), initial Cd(II) concentration (25 mg/L), speed agitation 100 rpm, and pH (7.6). It was observed that the percentage removal of Cd(II) ions was improved sharply from 52% to 93.6% with an increasing amount of adsorbent from 5 mg to 10 mg, respectively, due to increasing the availability of active adsorption sites on the Fe_3O_4@CS@DMSA surface. Conversely, the adsorption capacity of Fe_3O_4@CS@DMSA nanocomposite toward Cd(II) reduced from 65.0 to 58.5 mg/g with rising the amount of Fe_3O_4@CS@DMSA adsorbent to 10 mg. This is due to the adsorption capacity being inversely proportional to the adsorbent mass as per equation (Equation (1)) [38, 52]. After the adsorbent mass of 10 mg, no significant change in adsorption capacity was observed.

3.2.3. Effect of Contact Time. To find out the optimum contact time, experiments were conducted at various time intervals between 5 and 350 min at constant adsorbent mass (10 mg), initial Cd(II) concentration (25 mg/L), pH (7.6), stirring rate (100 rpm), and temperature (25°C) as presented in Figure 4(c). It was noticed that the amount of Cd(II) adsorbed onto the Fe_3O_4@CS@DMSA increased rapidly with increasing equilibrium time and the maximum adsorption capacity and removal efficiency reached up to 58.0 mg/g and 92.8%, respectively, at 210 min. In the initial stage of the adsorption process, the Cd(II) ions easily interacted with active sites of Fe_3O_4@CS@DMSA nanocomposite owing to the abundance of the active adsorption sites on the Fe_3O_4@CS@DMSA surface. After 210 min, no significant change in the adsorption capacity owing to the active sites of Fe_3O_4@CS@DMSA tended to saturate and could not easily adsorb the Cd(II) ions.

3.2.4. Effect of Initial Cd(II) Concentration and Temperatures. Figure 4(d) displays the influence of initial Cd(II) adsorption in the range of 25 to 300 mg/L with different temperatures (298-318 K) on the adsorption capacity of Fe_3O_4@CS@DMSA toward Cd(II) ions at constant of the other parameters (pH = 7.6, adsorbent mass = 10 mg, agitation speed = 100 rpm, and contact time = 210 min). The amount of Cd(II) adsorbed onto the Fe_3O_4@CS@DMSA increased from 57.5 to 295 mg/g with the rising initial Cd(II) ion concentration from 25 to 300 mg/L at 298 K. This phenomenon can be explained that a higher Cd(II) concentration rises the driving force and provides more collisions between Cd(II) ions and active sites of Fe_3O_4@CS@DMSA which could improve the adsorption rate. The influence of temperature on the adsorption process is presented in Figure 4(b). The adsorption capacity of Fe_3O_4@CS@DMSA toward Cd(II) was decreased from 295 to 195 mg/g when the temperature was improved from 298 K to 318 K at 300 mg/L, suggesting that the adsorption of Cd(II) on Fe_3O_4@CS@DMSA is exothermic. This could be explained by the weakening of the adsorptive forces between the active sites of Fe_3O_4@CS@DMSA nanocomposite and the Cd(II) ions [53], which is consistent with the previous report on Cd(II) adsorption by MGO-Trp [54] and CSAP [55].

Table 2: Isotherm data for Cd(II) adsorption by Fe_3O_4@CS@DMSA nanocomposite (time: 210 min; C_o: 25-300 mg/L; adsorbent dose: 0.01 g; agitation speed: 100 rpm).

Model	Cd(II) 298 K	308 K	318 K
Langmuir			
q_m (mg/g)	314.12	302.73	258.73
K_L (L/mg)	0.0698	0.0278	0.0151
R_L	0.3541	0.5897	0.7254
R^2	0.96915	0.97306	0.97069
Freundlich			
K_f (mg/g) $(L/mg)^{1/n}$	65.213	36.361	18.691
n	3.2730	2.6270	2.2381
R^2	0.96072	0.95405	0.96607
Dubinin-R			
q_s (mg/g)	261.86	231.17	182.33
$K_{D\text{-}R}$ (mol^2 KJ^{-2})	15.900	115.32	318.78
E (kJ mol^{-1})	0.1773	0.0658	0.0396
R^2	0.7983	0.82341	0.8159

3.3. Modeling

3.3.1. Isotherm Model. The adsorption of studied Cd(II) onto Fe_3O_4@CS@DMSA was studied at three various temperatures 298, 308, and 318 K by different nonlinear isotherm models, namely, Dubinin Radushkevich (Equations (4)–(6)) [56], Langmuir (Equation (7)) [57], Freundlich (Equation (8)) [58], and models. The fitting outcomes and parameters are indicated in Figure 5 and Table 2, respectively.

$$q_e = q_s\, e^{-K_{D\text{-}R}\,\varepsilon^2}, \tag{4}$$

$$\varepsilon = \mathrm{RTln}\left(1 + \frac{1}{C_e}\right), \tag{5}$$

Table 3: Comparison of Cd(II) adsorption performance on Fe_3O_4@CS@DMSA nanocomposite with different adsorbents.

Adsorbent	Kinetic models	Isotherm models	q_m (mg/g)	Reference
Fe_3O_4/chitosan-glycine-PEGDE	Pseudo-second-order	Langmuir	171.06	[61]
Polyethyleneimine-modified magnetic porous cassava	Pseudo-second-order	Langmuir	143.6	[62]
Chitosan-modified kiwi branch biochar	Pseudo-second-order	Langmuir	126.58	[63]
Sulfhydryl-modified chitosan beads	Pseudo-second-order	Langmuir	183.1	[64]
MNP-DMSA	Pseudo-first-order	Langmuir	25.44	[65]
Chitosan-pectin gel beads	Pseudo-second-order	Langmuir	177.6	[66]
Chitosan-iron oxide (CS-Fe_2O_3)	Pseudo-second-order	Langmuir	204.318	[67]
Thiocarbohydrazide-chitosan gel	Pseudo-second-order	Langmuir	81.26	[68]
Fe_3O_4@CS@DMSA	Pseudo-first-order	Langmuir	314.12	This study

$$E = \frac{1}{\sqrt{2K_{\text{D-R}}}}, \tag{6}$$

$$q_e = \frac{q_m K_L C_e}{1 + K_L C_e}, \tag{7}$$

$$q_e = K_F C_e^{1/n}, \tag{8}$$

where C_e (mg/g) is the equilibrium aqueous-phase Cd(II) concentration. q_e and q_m refer to the equilibrium and maximum amount of Cd(II) adsorbed (mg/g), respectively; K_{DR} (mol^2/kJ^2), K_F, and K_L are the constants of D-R, Freundlich, and Langmuir models, respectively; E (kJ/mol) and ε are the average free energy and the Polanyi potential, respectively; n is the adsorption intensity.

Figure 5 displays the three nonlinear fitting parameter results of the adsorption isotherm models for the Cd(II) adsorption on Fe_3O_4@CS@DMSA nanocomposite. By comparison, it was observed that the R^2 values were 0.96215, 0.97072, and 0.7983 for Langmuir, Freundlich, and D-R isotherms, respectively. Thus, the experimental data was better described by the Freundlich ($R^2 = 0.97072$) model than those of the Langmuir and D-R models, which indicated the heterogeneous nature of Fe_3O_4@CS@DMSA and a contribution of electrostatic interaction to the Cd(II) adsorption on Fe_3O_4@CS@DMSA (physisorption nature) [59]. By applying the Freundlich equation, the values of n (adsorption intensity) were in the range of 2.2381-3.2730, indicating that multilayer adsorption occurred onto the heterogeneous surface of Fe_3O_4@CS@DMSA. In addition, the Cd(II) adsorption is a favorable process. The higher value of $n = 3.2730$ at 298 K indicates that the Fe_3O_4@CS@DMSA nanocomposite has better adsorption performance [59, 60]. According to the Langmuir model, the maximum amount of Cd(II) adsorbed was 314.12 mg/g. This value is higher than other material adsorbents for adsorption of Cd(II) like Fe_3O_4/chitosan-glycine-PEGDE (171.06) [61], polyethyleneimine-modified magnetic porous cassava (143.6) [62], chitosan-modified kiwi branch biochar (126.58) [63], sulfhydryl-modified chitosan beads (183.1) [64], MNP-DMSA (25.44) [65], chitosan-pectin gel beads (177.6) [66], chitosan-iron oxide (CS-Fe_2O_3) (204.318) [67], and thiocarbohydrazide-chitosan gel (81.26) [68] (Table 3). According to the D-R isotherm, the values of means free energy (E) were found to be in the range of 0.0396-0.1773 kJ/mol), which indicated that the Cd(II) adsorption onto Fe_3O_4@CS@DMSA nanocomposite classified as a physical adsorption process due to the E value is less than 8 kJ/mol [69].

Table 4: Kinetic data for Cd(II) adsorption by Fe_3O_4@CS@DMSA nanocomposite (T: 298 K; C_o: 25 mg/L; adsorbent dose: 0.01 g; agitation speed: 100 rpm).

Model	Parameters C_o: 25 mg/L, $q_{e,\text{exp.}}$: 58.75 mg/g	Value
Pseudo-first-order	$q_{e1,\text{cal.}}$ (mg/g)	61.45
	K_1 (1/min)	0.0103
	R^2	0.97515
Pseudo-second-order	$q_{e2,\text{cal.}}$ (mg/g)	79.82
	K_2 (g/mg-min)	0.00011
	R^2	0.9567
Elovich	A (mg/g min)	0.87664
	B (mg/g)	0.04278
	R^2	0.93427

3.3.2. Kinetic Model. The kinetic studies were estimated at different contact times in the range of 5-350 min with fixed parameter conditions (pH = 7.6, initial Cd(II) concentration (25 mg/L), adsorbent mass = 10 mg, contact time = 210 min, and temperature = 298 K). Three nonlinear kinetic models, namely, Elovich (Equation (9)) [70], pseudo-first-order (PFO) (Equation (10)) [71], and pseudo-second-order (PSO) (Equation (11)) models, were applied to understand the mechanism of Cd(II) adsorption on Fe_3O_4@CS@DMSA nanocomposite. The fitting results and parameters are indicated in Figure 5(d) and Table 4, respectively.

$$q_t = \frac{1}{\beta} \ln(1 + \alpha\beta t), \tag{9}$$

$$q_q = q_e\left(1 - e^{-k_1 t}\right), \tag{10}$$

$$q_t = \frac{q_e^2 k_2 t}{1 + q_e k_2 t}, \tag{11}$$

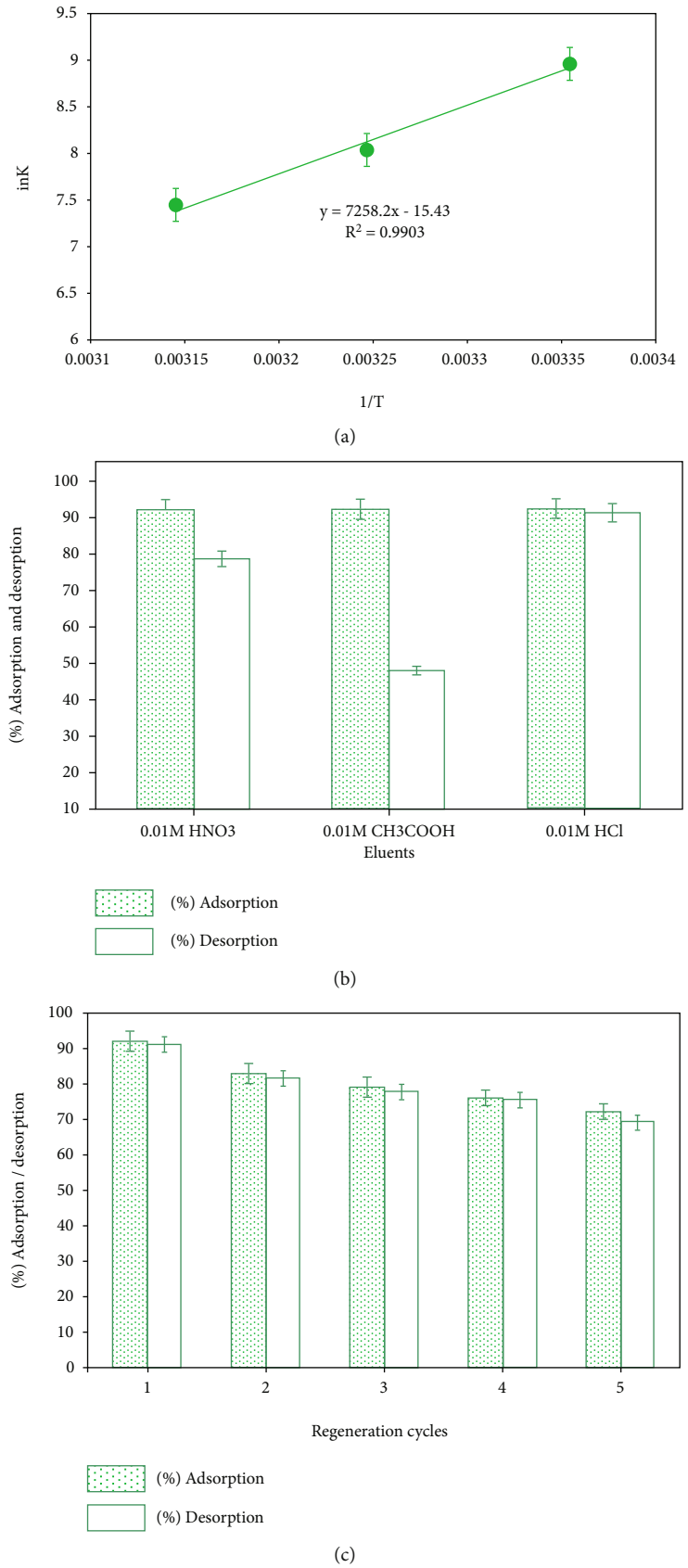

Figure 6: (a) Van't Hoff plot for the adsorption of Cd(II), (b) comparison of eluents for desorption of Cd(II) from Fe_3O_4@CS@DMSA surface, and (c) reusability of Fe_3O_4@CS@DMSA.

Table 5: Thermodynamic data for the Cd(II) adsorption on Fe_3O_4@CS@DMSA.

Metal ions	ΔH° (kJ/mol)	ΔS° (J/mol·K)	ΔG° (kJ/mol)		
			298 K	308 K	318 K
Cd(II)	-60.344	-128.280	-22.220	-20.608	-19.668

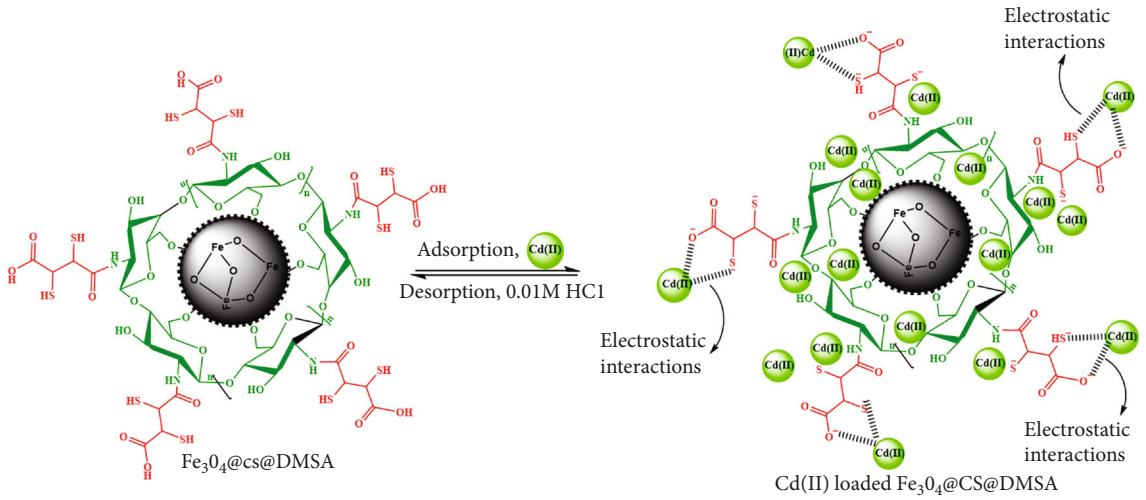

Figure 7: Mechanism adsorption of Cd(II) onto Fe_3O_4@CS@DMSA nanocomposite.

where q_e and q_t (mg/g) refer to the amounts of Cd(II) adsorbed on Fe_3O_4@CS@DMSA at equilibrium and time t, respectively; k_1 is the PFO rate constant; k_2 represents the PSO rate constant; β (mg/g) is the Elovich kinetic parameter; α refers to the desorption constant.

Based on R^2 values, PFO displays a better correlation coefficient ($R^2 = 0.97515$) than the PSO ($R^2 = 0.9567$) and Elovich ($R^2 = 0.93427$) models, suggesting the rate-limiting step for Cd(II) is physisorption involving electrostatic interaction between Cd(II) and Fe_3O_4@CS@DMSA nanocomposite. The value of $q_{e.\mathrm{cal}}$ (61.45 mg/g) calculated is close to the experimental equilibrium adsorption capacities ($q_{e,\mathrm{exp}} = 58.75$ mg/g). By applying the Elovich equation, the values of α and β were 0.877 mg/g min and 0.043 mg/g with R^2 (0.93427), respectively. The low value of R^2 indicates the absence of a chemisorption mechanism.

3.3.3. Adsorption Thermodynamics. The thermodynamic parameters, namely, enthalpy change (ΔH°) (Equation (12) and entropy change (ΔS°) (Equation (12)), can be obtained from the slope and intercept of the Van't Hoff plot of ln K_e vs. $1/T$ (Figure 6(a)) at different temperatures (298-318 K), and the free energy change (ΔG°) can be estimated from the equation (Equation (13)):

$$\ln K_e^0 = -\frac{\Delta H^\circ}{\mathrm{RT}} + \frac{\Delta S^\circ}{R}, \tag{12}$$

$$\Delta G^\circ = -\mathrm{RT}\ \ln K_e^0, \tag{13}$$

$$K_e^0 = \frac{(1000 \cdot K_L \text{ molecular weight of adsorbate}) \cdot [\text{adsorbate}]^\circ}{\gamma}, \tag{14}$$

where K_e^0 (Equation (14)) is the thermodynamic equilibrium constant at a certain temperature [59–61] and [adsorbate]°, γ, and K_L are the standard concentrations of the adsorbate (1.0 mol/L), activity coefficient, and Langmuir constant, respectively. The thermodynamic parameters for Cd(II) adsorption onto Fe_3O_4@CS@DMSA are summarized in Table 5. The negative values of free energy (ΔG°) was noticed, indicating that the Cd(II) adsorption onto Fe_3O_4@CS@DMSA is a spontaneous reaction and the values of ΔG° were increased from -22.36 to -19.66 kJ/mol with rising temperature from 298 to 318 K which demonstrates the favorability of the adsorption of Cd(II) at a lower temperature. Negative values of ΔH° and ΔS° indicated that the Cd(II) adsorption onto Fe_3O_4@CS@DMSA was exothermic and the decreased the reaction randomness.

3.4. Adsorption Mechanism. The proposed adsorption mechanism is shown in Figure 7. Based on the adsorption kinetic results, the adsorption process followed the pseudo-first-order model, suggesting a physical interaction through electrostatic attraction between the Cd(II) ions and the Fe_3O_4@CS@DMSA nanocomposite. According to the FTIR analysis (Figure 1(a)), the position peaks of functional groups declined in intensity and slightly shifted to a lower wavenumber. In detail, the bands at 3393 and 2550 cm^{-1} decrease in intensity owing to the interaction between Cd(II) and carboxyl (COOH), hydroxyl (OH), and SH groups, respectively, on the Fe_3O_4@CS@DMSA surface by electrostatic interaction. In addition, the band at 1274 cm^{-1} for ν (C-O) disappeared after Cd(II) adsorption onto the Fe_3O_4@CS@DMSA surface. The decreased intensity of the band at 1481 cm^{-1} for $\nu(\mathrm{COO}^-)$ indicates the adsorption of Cd(II) onto the Fe_3O_4@CS@DMSA surface. Besides, the

Fe_3O_4@CS@DMSA exhibited a high adsorption capacity of Cd(II) owing to the presence of functional moieties (SH, COOH, OH, and NH_2) on the surface of Fe_3O_4@CS@DMSA, which was confirmed by the FTIR spectrum. The EDX analysis displays a new peak of Cd(II), which indicates Cd(II) ion adsorption onto the Fe_3O_4@CS@DMSA surface.

3.5. Reusability Study. To evaluate the reusability of the Fe_3O_4@CS@DMSA, adsorption and desorption tests were conducted using three eluents, namely, 0.01 M CH_3COOH, 0.01 M HNO_3, and 0.01 M HCL. The % desorption (Equation (15)) was estimated by the equation:

$$\%\text{desorption} = \frac{C_m}{C_e} \times 100, \tag{15}$$

where C_m and C_e (mg/L) refer to the concentration of Cd(II) ion released in the solution and the initially adsorbed Cd(II) concentration, respectively. The results of the Cd(II) adsorption/desorption test on Fe_3O_4@CS@DMSA nanocomposite using eluents are indicated in Figure 6(b). It was observed that the percentage desorption was found to be CH_3COOH (47.48%), HNO_3 (87.26%), and HCl (91.3%), which indicate the best eluent for desorption of Cd(II) was 0.01 M HCl owing to the smaller ionic size of the Cl^- ion compared to CH_3COO^- and NO_3^-. For reusability of the Fe_3O_4@CS@DMSA study, the Cd(II)-loaded Fe_3O_4@CS@DMSA was isolated using a magnet and then the solid adsorbent was washed with deionized water, dried, and regenerated with 25 mL of 0.01 M HCl. After that, the sample was shaken at room temperature for 210 min. The solid/solution phase is separated via a magnet, and the supernatants are analyzed by the AAS method. After desorption, the Fe_3O_4@CS@DMSA nanocomposite was reused to Cd(II) adsorption and five adsorption/desorption cycles were applied. The results obtained are presented in Figure 6(c). It is seen that up to five cycles about 72% of Cd(II) were successfully removed. The reduction in removal efficiency of Cd(II) after five cycles may be owing to incomplete desorption of the Cd(II) ions on Fe_3O_4@CS@DMSA.

4. Conclusion

Fe_3O_4@CS@DMSA nanocomposite was synthesized via the in situ coprecipitation method followed by a covalent functionalization of Fe_3O_4@CS with DMSA acid by amidation reaction. The synthesized Fe_3O_4@CS@DMSA nanocomposite was characterized using zeta potential, FTIR, XRD, TEM, EDX, and TGA techniques. These techniques confirmed the formation of adsorbent successfully. After characterization, the Fe_3O_4@CS@DMSA was used to eliminate Cd(II) ions from aqueous systems. The Fe_3O_4@CS@DMSA adsorbent exhibited a high adsorption capacity (314.12 mg/g at the optimum condition pH: 7.6, contact time: 210 min, temperature: 298 K, adsorbent mass:10 mg, and stirring rate: 100 rpm). The FTIR and EDX results confirmed the existence of Cd(II) ions after adsorption on Fe_3O_4@CS@DMSA nanocomposite. The Freundlich isotherm data and pseudo-first-order kinetic data displayed more compatibility with the equilibrium data than that of other models. The mechanism of Cd(II) adsorption on Fe_3O_4@CS@DMSA nanocomposite is electrostatic attraction. The thermodynamic results confirmed the spontaneous and exothermic nature of adsorption. The reusability test of Fe_3O_4@CS@DMSA nanocomposite exhibited that the adsorption efficiency was 72% after five cycles. The results indicate that the Fe_3O_4@CS@DMSA has a good potential for the elimination of Cd(II) from an aqueous solution.

Data Availability

Anyone who wants to request research article data can contact me directly via the following email: aalkudami@ksu.edu.sa, aaaayoub17@gmail.com, Chemistry Department, College of Science, King Saud University.

Conflicts of Interest

There are no conflicts to declare.

Acknowledgments

The authors are thankful to the Deanship of Scientific Research at Najran University for funding this work under the General Research Funding program grant code (NU/-/SERC/10/509).

References

[1] C. Zhang, Z. Chen, Y. Tao et al., "Enhanced removal of trichlorfon and Cd(II) from aqueous solution by magnetically separable chitosan beads immobilized _Aspergillus sydowii_," *International Journal of Biological Macromolecules*, vol. 148, pp. 457–465, 2020.

[2] X. Xie, X. Zhao, X. Luo et al., "Mechanically activated starch magnetic microspheres for Cd(II) adsorption from aqueous solution," *Chinese Journal of Chemical Engineering*, vol. 33, pp. 40–49, 2021.

[3] P. Zong, Y. Cheng, S. Wang, and L. Wang, "Simultaneous removal of Cd(II) and phenol pollutions through magnetic graphene oxide nanocomposites coated polyaniline using low temperature plasma technique," *International Journal of Hydrogen Energy*, vol. 45, no. 38, pp. 20106–20119, 2020.

[4] H. Zhang, Q. Dang, C. Liu et al., "Fabrication of methyl acrylate and tetraethylenepentamine grafted magnetic chitosan microparticles for capture of Cd(II) from aqueous solutions," *Journal of Hazardous Materials*, vol. 366, pp. 346–357, 2019.

[5] A. Ramos-Ruiz, J. V. Wilkening, J. A. Field, and R. Sierra-Alvarez, "Leaching of cadmium and tellurium from cadmium telluride (CdTe) thin-film solar panels under simulated landfill conditions," *Journal of Hazardous Materials*, vol. 336, pp. 57–64, 2017.

[6] H. Wu, W. Wang, Y. Huang et al., "Comprehensive evaluation on a prospective precipitation-flotation process for metal-ions removal from wastewater simulants," *Journal of Hazardous Materials*, vol. 371, pp. 592–602, 2019.

[7] M. Alqadami, M. Naushad, T. Ahamad, A. Algamdi, H. Alshahrani, and S. K. S. Usluc, "Removal of highly toxic Cd(II) metal ions from aqueous medium using magnetic nanocomposite: adsorption kinetics, isotherm and thermodynamics," *Desalination and Water Treatment*, vol. 181, pp. 355–361, 2020.

[8] C. Y. Foong, M. D. H. Wirzal, and M. A. Bustam, "A review on nanofibers membrane with amino-based ionic liquid for heavy metal removal," *Journal of Molecular Liquids*, vol. 297, article 111793, 2020.

[9] S. M. Hosseini, H. Alibakhshi, E. Jashni et al., "A novel layer-by-layer heterogeneous cation exchange membrane for heavy metal ions removal from water," *Journal of Hazardous Materials*, vol. 381, article 120884, 2020.

[10] A. Karatutlu, A. Barhoum, and A. Sapelkin, "Liquid-phase synthesis of nanoparticles and nanostructured materials," in *Emerging Applications of Nanoparticles and Architecture Nanostructures*, pp. 1–28, Elsevier, 2018.

[11] F.-M. Allioux, P. Kapruwan, N. Milne et al., "Electro-capture of heavy metal ions with carbon cloth integrated microfluidic devices," *Separation and Purification Technology*, vol. 194, pp. 26–32, 2018.

[12] X. Li, Y. Qi, Y. Li, Y. Zhang, X. He, and Y. Wang, "Novel magnetic beads based on sodium alginate gel crosslinked by zirconium(IV) and their effective removal for Pb^{2+} in aqueous solutions by using a batch and continuous systems," *Bioresource Technology*, vol. 142, pp. 611–619, 2013.

[13] W. Yu, J. Hu, Y. Yu et al., "Facile preparation of sulfonated biochar for highly efficient removal of toxic Pb(II) and Cd(II) from wastewater," *Science of the Total Environment*, vol. 750, article 141545, 2021.

[14] J. Qu, X. Tian, Z. Jiang et al., "Multi-component adsorption of Pb(II), Cd(II) and Ni(II) onto microwave- functionalized cellulose: kinetics, isotherms, thermodynamics, mechanisms and application for electroplating wastewater purification," *Journal of Hazardous Materials*, vol. 387, article 121718, 2020.

[15] A. L. Popovic, J. D. Rusmirovic, Z. Velickovic et al., "Kinetics and column adsorption study of diclofenac and heavy-metal ions removal by amino-functionalized lignin microspheres," *Journal of Industrial and Engineering Chemistry*, vol. 93, pp. 302–314, 2021.

[16] D. Roy, S. Neogi, and S. De, "Adsorptive removal of heavy metals from battery industry effluent using MOF incorporated polymeric beads: a combined experimental and modeling approach," *Journal of Hazardous Materials*, vol. 403, article 123624, 2021.

[17] A. Shahbazi, N. N. Marnani, and Z. Salahshoor, "Synergistic and antagonistic effects in simultaneous adsorption of Pb(II) and Cd(II) from aqueous solutions onto chitosan functionalized EDTA-silane/mGO," *Biocatalysis and Agricultural Biotechnology*, vol. 22, article 101398, 2019.

[18] M. Naushad, A. A. Alqadami, A. A. Al-Kahtani, T. Ahamad, M. R. Awual, and T. Tatarchuk, "Adsorption of textile dye using para-aminobenzoic acid modified activated carbon: kinetic and equilibrium studies," *Journal of Molecular Liquids*, vol. 296, p. 112075, 2019.

[19] S. Melhi, M. Algamdi, A. A. Alqadami, M. A. Khan, and E. H. Alosaimi, "Fabrication of magnetically recyclable nanocomposite as an effective adsorbent for the removal of malachite green from water," *Chemical Engineering Research and Design*, vol. 177, pp. 843–854, 2022.

[20] Z. Zhang, T. Wang, H. Zhang, Y. Liu, and B. Xing, "Adsorption of Pb(II) and Cd(II) by magnetic activated carbon and its mechanism," *Science of the Total Environment*, vol. 757, article 143910, 2021.

[21] S. M. Ghasemabadi, M. Baghdadi, E. Safari, and F. Ghazban, "Investigation of continuous adsorption of Pb(II), As(III), Cd(II), and Cr(VI) using a mixture of magnetic graphite oxide and sand as a medium in a fixed-bed column," *Journal of Environmental Chemical Engineering*, vol. 6, no. 4, pp. 4840–4849, 2018.

[22] H. Xu, H. Yuan, J. Yu, and S. Lin, "Study on the competitive adsorption and correlational mechanism for heavy metal ions using the carboxylated magnetic iron oxide nanoparticles (MNPs- COOH) as efficient adsorbents," *Applied Surface Science*, vol. 473, pp. 960–966, 2019.

[23] I. Anastopoulos, A. Bhatnagar, D. N. Bikiaris, and G. Z. Kyzas, "Chitin adsorbents for toxic metals: a review," *International Journal of Molecular Sciences*, vol. 18, no. 1, p. 114, 2017.

[24] A. E. Awad, *Removal of Fe and Cu ions from aqueous solutions by adsorption using peanut hulls*, 2017.

[25] T. Liu, X. Yang, Z.-L. Wang, and X. Yan, "Enhanced chitosan beads-supported Fe^0-nanoparticles for removal of heavy metals from electroplating wastewater in permeable reactive barriers," *Water Research*, vol. 47, no. 17, pp. 6691–6700, 2013.

[26] M. Ahmad, B. Zhang, J. Wang et al., "New method for hydrogel synthesis from diphenylcarbazide chitosan for selective copper removal," *International Journal of Biological Macromolecules*, vol. 136, pp. 189–198, 2019.

[27] Y. Xiang, Z. Bai, S. Zhang et al., "Lead adsorption, anticoagulation and in vivo toxicity studies on the new magnetic nanomaterial Fe_3O_4@SiO_2@DMSA as a hemoperfusion adsorbent," *Nanomedicine: Nanotechnology, Biology and Medicine*, vol. 13, pp. 1341–1351, 2017.

[28] I. Pavlovic, M. R. Pérez, C. Barriga, and M. A. Ulibarri, "Adsorption of Cu^{2+}, Cd^{2+} and Pb^{2+} ions by layered double hydroxides intercalated with the chelating agents diethylenetriaminepentaacetate and meso-2,3-dimercaptosuccinate," *Applied Clay Science*, vol. 43, no. 1, pp. 125–129, 2009.

[29] J. J. Chisolm, "Safety and efficacy of meso-2,3-dimercaptosuccinic acid (DMSA) in children with elevated blood lead concentrations," *Journal of Toxicology: Clinical Toxicology*, vol. 38, no. 4, pp. 365–375, 2000.

[30] A. Sari, M. Tuzen, D. Citak, and M. Soylak, "Equilibrium, kinetic and thermodynamic studies of adsorption of Pb(II) from aqueous solution onto Turkish kaolinite clay," *Journal of Hazardous Materials*, vol. 149, no. 2, pp. 283–291, 2007.

[31] E. Sevinç, F. S. Ertas, G. Ulusoy, C. Ozen, and H. Y. Acar, "Meso-2,3-dimercaptosuccinic acid: from heavy metal chelation to CdS quantum dots," *Journal of Materials Chemistry*, vol. 22, no. 11, pp. 5137–5144, 2012.

[32] S. Lotfi, F. Ghaderi, A. Bahari, and S. Mahjoub, "Preparation and characterization of magnetite–chitosan nanoparticles and evaluation of their cytotoxicity effects on MCF7 and fibroblast cells," *Journal of Superconductivity and Novel Magnetism*, vol. 30, no. 12, pp. 3431–3438, 2017.

[33] M. Alsuhybani, A. Alshahrani, M. Algamdi, A. A. Al-Kahtani, and A. A. Alqadami, "Highly efficient removal of Pb(II) from aqueous systems using a new nanocomposite: adsorption, isotherm, kinetic and mechanism studies," *Journal of Molecular Liquids*, vol. 301, article 112393, 2020.

[34] H. Zhai, Y. Wang, M. Wang et al., "Construction of a glutathione-responsive and silica-based nanocomposite for controlled release of chelator dimercaptosuccinic acid," *International Journal of Molecular Sciences*, vol. 19, no. 12, p. 3790, 2018.

[35] L. Fan, M. Deng, C. Lin et al., "A multifunctional composite Fe_3O_4/MOF/l-cysteine for removal, magnetic solid phase

extraction and fluorescence sensing of Cd(ii)," *RSC Advances*, vol. 8, no. 19, pp. 10561–10572, 2018.

[36] M. K. Jaiswal, R. Banerjee, P. Pradhan, and D. Bahadur, "Thermal behavior of magnetically modalized poly(_N_ -isopropylacrylamide)-chitosan based nanohydrogel," *Colloids and Surfaces B: Biointerfaces*, vol. 81, no. 1, pp. 185–194, 2010.

[37] N. F. Abd Razak, M. Shamsuddin, and S. L. Lee, "Adsorption kinetics and thermodynamics studies of gold(III) ions using thioctic acid functionalized silica coated magnetite nanoparticles," *Chemical Engineering Research and Design*, vol. 130, pp. 18–28, 2018.

[38] A. M. Aldawsari, I. H. Alsohaimi, A. A. Al-Kahtani, A. A. Alqadami, Z. E. Ali Abdalla, and E. A. M. Saleh, "Adsorptive performance of aminoterephthalic acid modified oxidized activated carbon for malachite green dye: mechanism, kinetic and thermodynamic studies," *Separation Science and Technology*, vol. 56, no. 5, pp. 835–846, 2021.

[39] A. Amiri, M. Shanbedi, M. Savari, B. T. Chew, and S. N. Kazi, "Cadmium ion sorption from aqueous solutions by high surface area ethylenediaminetetraacetic acid- and diethylene triamine pentaacetic acid-treated carbon nanotubes," *RSC Advances*, vol. 5, no. 87, pp. 71144–71152, 2015.

[40] B. Chen, Y. Liu, S. Chen, X. Zhao, W. Yue, and X. Pan, "Nitrogen-rich core/shell magnetic nanostructures for selective adsorption and separation of anionic dyes from aqueous solution," *Environmental Science: Nano*, vol. 3, no. 3, pp. 670–681, 2016.

[41] S. Shahraki, H. S. Delarami, and F. Khosravi, "Synthesis and characterization of an adsorptive Schiff base-chitosan nanocomposite for removal of Pb(II) ion from aqueous media," *International Journal of Biological Macromolecules*, vol. 139, pp. 577–586, 2019.

[42] J. Safari and L. Javadian, "Chitosan decorated Fe_3O_4nanoparticles as a magnetic catalyst in the synthesis of phenytoin derivatives," *RSC Advances*, vol. 4, no. 90, pp. 48973–48979, 2014.

[43] M. A. Zulfikar, S. Afrita, D. Wahyuningrum, and M. Ledyastuti, "Preparation of Fe_3O_4-chitosan hybrid nanoparticles used for humic acid adsorption," *Environmental Nanotechnology, Monitoring & Management*, vol. 6, pp. 64–75, 2016.

[44] I.-C. Masthoff, M. Kraken, D. Menzel, F. J. Litterst, and G. Garnweitner, "Study of the growth of hydrophilic iron oxide nanoparticles obtained via the non-aqueous sol–gel method," *Journal of Sol-Gel Science and Technology*, vol. 77, no. 3, pp. 553–564, 2016.

[45] P. Gogoi, A. J. Thakur, R. R. Devi, B. Das, and T. K. Maji, "Adsorption of As(V) from contaminated water over chitosan coated magnetite nanoparticle: equilibrium and kinetics study," *Environmental Nanotechnology, Monitoring & Management*, vol. 8, pp. 297–305, 2017.

[46] A. A. Alqadami, M. Naushad, Z. A. ALOthman, M. Alsuhybani, and M. Algamdi, "Excellent adsorptive performance of a new nanocomposite for removal of toxic Pb(II) from aqueous environment: adsorption mechanism and modeling analysis," *Journal of Hazardous Materials*, vol. 389, p. 121896, 2020.

[47] A. A. Alqadami, M. A. Khan, M. Otero, M. R. Siddiqui, B.-H. Jeon, and K. M. Batoo, "A magnetic nanocomposite produced from camel bones for an efficient adsorption of toxic metals from water," *Journal of Cleaner Production*, vol. 178, pp. 293–304, 2018.

[48] H. Nguyen Van, H. Chu Van, T. Luu Hoang, D. K. Vo Nguyen, and C. N. Ha Thuc, "The starch modified montmorillonite for the removal of Pb(II), Cd(II) and Ni(II) ions from aqueous solutions," *Arabian Journal of Chemistry*, vol. 13, no. 9, pp. 7212–7223, 2020.

[49] J. Li, C. Chen, K. Zhu, and X. Wang, "Nanoscale zero-valent iron particles modified on reduced graphene oxides using a plasma technique for Cd(II) removal," *Journal of the Taiwan Institute of Chemical Engineers*, vol. 59, pp. 389–394, 2016.

[50] S. Bao, W. Yang, Y. Wang, Y. Yu, and Y. Sun, "One-pot synthesis of magnetic graphene oxide composites as an efficient and recoverable adsorbent for Cd(II) and Pb(II) removal from aqueous solution," *Journal of Hazardous Materials*, vol. 381, article 120914, 2020.

[51] C. Sun, Y. Xie, X. Ren et al., "Efficient removal of Cd(II) by core-shell Fe_3O_4@polydopamine microspheres from aqueous solution," *Journal of Molecular Liquids*, vol. 295, p. 111724, 2019.

[52] Y. Geng, J. Zhang, J. Zhou, and J. Lei, "Study on adsorption of methylene blue by a novel composite material of $TiO_2$and alum sludge," *RSC Advances*, vol. 8, no. 57, pp. 32799–32807, 2018.

[53] H. S. Hassan, M. F. Elkady, A. A. Farghali, A. M. Salem, and A. I. A. El-Hamid, "Fabrication of novel magnetic zinc oxide cellulose acetate hybrid nano-fiber to be utilized for phenol decontamination," *Journal of the Taiwan Institute of Chemical Engineers*, vol. 78, pp. 307–316, 2017.

[54] M. E. Mahmoud, M. M. Osman, H. Abdel-Aal, and G. M. Nabil, "Microwave-assisted adsorption of Cr(VI), Cd(II) and Pb(II) in presence of magnetic graphene oxide-covalently functionalized-tryptophan nanocomposite," *Journal of Alloys and Compounds*, vol. 823, article 153855, 2020.

[55] M. Monier, D. M. Ayad, and D. A. Abdel-Latif, "Adsorption of Cu(II), Cd(II) and Ni(II) ions by cross-linked magnetic chitosan-2-aminopyridine glyoxal Schiff's base," *Colloids and Surfaces B: Biointerfaces*, vol. 94, pp. 250–258, 2012.

[56] M. M. Dubinin and L. V. Radushkevich, "Equation of the characteristic curve of activated charcoal," *Proceedings of the Academy of Sciences of the USSR, Physical Chemistry Section*, vol. 1, p. 857, 1947.

[57] A. Wallis and M. F. Dollard, "Local and global factors in work stress - the Australian dairy farming examplar," *Scandinavian Journal of Work, Environment & Health*, vol. 34, pp. 66–74, 2008.

[58] F. Herbert, "Über die "Adsorption in Lösungen"," *Zeitschrift für Physikalische Chemie*, vol. 57U, no. 1, pp. 385–470, 1907.

[59] Z. Chai, C. Li, Y. Zhu et al., "Arginine-modified magnetic chitosan: preparation, characterization and adsorption of gallic acid in sugar solution," *International Journal of Biological Macromolecules*, vol. 165, no. Part A, pp. 506–516, 2020.

[60] K. Yang, Z. Lou, R. Fu et al., "Multiwalled carbon nanotubes incorporated with or without amino groups for aqueous Pb(II) removal: comparison and mechanism study," *Journal of Molecular Liquids*, vol. 260, pp. 149–158, 2018.

[61] J. Rahmi, Julinawati, M. Nina, H. Fathana, and M. Iqhrammullah, "Preparation and characterization of new magnetic chitosan-glycine-PEGDE (Fe_3O_4/Ch-G-P) beads for aqueous Cd(II) removal," *Journal of Water Process Engineering*, vol. 45, p. 102493, 2022.

[62] X. Xie, L. Zhang, X. Luo et al., "PEI modified magnetic porous cassava residue microspheres for adsorbing Cd(II) from

aqueous solution," *European Polymer Journal*, vol. 159, article 110741, 2021.

[63] Y. Tan, X. Wan, X. Ni et al., "Efficient removal of Cd (II) from aqueous solution by chitosan modified kiwi branch biochar," *Chemosphere*, vol. 289, article 133251, 2022.

[64] Y. Yang, L. Zeng, Z. Lin, H. Jiang, and A. Zhang, "Adsorption of Pb^{2+}, Cu^{2+} and Cd^{2+} by sulfhydryl modified chitosan beads," *Carbohydrate Polymers*, vol. 274, article 118622, 2021.

[65] V. D. Chavan, V. P. Kothavale, S. C. Sahoo et al., "Adsorption and kinetic behavior of Cu(II) ions from aqueous solution on DMSA functionalized magnetic nanoparticles," *Physica B: Condensed Matter*, vol. 571, pp. 273–279, 2019.

[66] Z. Shao, J. Lu, J. Ding et al., "Novel green chitosan-pectin gel beads for the removal of Cu(II), Cd(II), Hg(II) and Pb(II) from aqueous solution," *International Journal of Biological Macromolecules*, vol. 176, pp. 217–225, 2021.

[67] R. Ahmad and A. Mirza, "Facile one pot green synthesis of chitosan-iron oxide (CS- Fe_2O_3) nanocomposite: removal of Pb(II) and Cd(II) from synthetic and industrial wastewater," *Journal of Cleaner Production*, vol. 186, pp. 342–352, 2018.

[68] R. Li, W. Liang, M. Li et al., "Removal of Cd(II) and Cr(VI) ions by highly cross-linked thiocarbohydrazide- chitosan gel," *International Journal of Biological Macromolecules*, vol. 104, no. Part A, pp. 1072–1081, 2017.

[69] S. Chowdhury and P. Saha, "Sea shell powder as a new adsorbent to remove basic green 4 (malachite green) from aqueous solutions: equilibrium, kinetic and thermodynamic studies," *Chemical Engineering Journal*, vol. 164, no. 1, pp. 168–177, 2010.

[70] S. Roginsky and Y. B. Zeldovich, "The catalytic oxidation of carbon monoxide on manganese dioxide," *Acta Physicochim. URSS*, vol. 1, p. 554, 1934.

[71] S. Lagergren, "About the theory of so-called adsorption of soluble substances," *The Hand*, vol. 24, pp. 1–39, 1898.